DJ-1 can form β-sheet structured aggregates that co-localize with pathological amyloid deposits

Katalin Solti[1^], Wei-Li Kuan[2^], Balázs Fórizs[3^], Gergely Kustos[3], Mihály Judith[4], Zoltán Varga[4], Balázs Herberth[3], Éva Moravcsik[3], Róbert Kiss[1], Manuela Kárpáti[3], Anna Mikes[1], Yanyan Zhao[5], Tímea Imre[6], Jean-Christophe Rochet[7], Franklin Aigbirhio[5], Caroline H. Williams-Gray[2], Roger A. Barker[2], Gergely Tóth[1,3,5*]

[1]*TTK-NAP B - Drug Discovery Research Group – Neurodegenerative Diseases, Institute of Organic Chemistry, Research Center for Natural Sciences, Budapest, Hungary*

[2]*John van Geest Centre for Brain Repair, Department of Clinical Neurosciences, University of Cambridge, Forvie Site, Robinson Way, Cambridge CB2 0PY, United Kingdom*

[3]*Cantabio Pharmaceuticals, Sunnyvale, California, USA*

[4]*Institute of Materials and Environmental Chemistry Research Centre for Natural Sciences, Budapest, Hungary*

[5]*Molecular Imaging Chemistry Laboratory, Wolfson Brain Imaging Centre, Department of Clinical Neurosciences, University of Cambridge, Cambridge CB2 0QQ, UK*

[6]*MS Metabolomic Research Laboratory, Institute of Organic Chemistry, Research Center for Natural Sciences, Budapest, Hungary*

[7]*Department of Medicinal Chemistry and Molecular Pharmacology and Purdue Institute for Integrative Neuroscience, Purdue University, West Lafayette, Indiana, USA*

^These authors equally contributed the study.

*Corresponding author email: toth.gergely@ttk.hu

Abstract

The loss of native function of the DJ-1 protein has been linked to the development of Parkinson's (PD) and other neurodegenerative diseases. Here we show that DJ-1 aggregates into β-sheet structured soluble and fibrillar aggregates *in vitro* under physiological conditions and that this process is promoted by the oxidation of its catalytic Cys106 residue. This aggregation resulted in the loss of its native biochemical glyoxalase function and in addition oxidized DJ-1 aggregates were observed to localize within Lewy bodies, neurofibrillary tangles and amyloid plaques in human PD and Alzheimer's (AD) patients' post-mortem brain tissue. These findings suggest that the aggregation of DJ-1 may be a critical player in the development of the pathology of PD and AD and demonstrate that loss of DJ-1 function can happen through DJ-1 aggregation. This could then contribute to AD and PD disease onset and progression.

Keywords: DJ-1 / Parkinson's / Alzheimer's / aggregation / amyloid

Introduction

The aggregation of proteins into soluble oligomers with a β-sheet structured core and amyloid fibrils[1, 2] is a pathological hallmark of many neurodegenerative diseases including Alzheimer's disease (AD)[3-5] and Parkinson's disease (PD)[6]. This aggregation process and the aggregated species generated by it can cause cellular degeneration[1] and are thought to be critical players in the pathogenic basis of these disorders.

DJ-1 is a multifunctional protein with various enzymatic functions involved in regulating redox and protein homeostasis[7], and its loss of function has been linked to the onset and progression of a wide range of diseases[7] including PD[8, 9], AD[10] and related disorders [10, 11] as well as stroke[12], type II diabetes[13, 14] and some types of cancer[15]. Specific mutations in the DJ-1 encoding gene, PARK7, cause familial autosomal recessive early-onset PD[8, 9] and, in some cases, amyotrophic lateral sclerosis[16] through structural destabilization of the protein. Under physiological conditions the active structural state of DJ-1 is a homodimer folded into seven beta-strands and nine helices per monomer[17]. Cys106 is an essential residue of DJ-1 responsible for its various functions[18] including a range of enzymatic activities such as glyoxalase[19], deglycase,[20] and protease[21] function. In addition, DJ-1 has been shown to function as a redox activated chaperone with the ability to inhibit α-synuclein aggregation[22, 23].

Cys106 is a highly reactive residue in DJ-I and can be oxidized from its native thiolate (-S-), to sulfinate ($-SO_2^-$), or sulfonate ($-SO_3^-$) state by oxidative stress[24]. The oxidation of DJ-1 at Cys106 has been observed in post-mortem brain samples in PD and AD patients[10] and in the red blood cells of PD patients[25], suggesting that this is associated with a diseased state[26].

DJ-1 has been observed to form aggregates *in vitro* and *in vivo*. Soluble high molecular weight aggregates of DJ-1 have been observed in PD patients' brain[27-29], and higher polymer

forms of oxidized DJ-1 have been detected specifically in unmedicated PD patients' erythrocytes[30], suggesting that the presence of such aggregates may have a link to a disease state. DJ-1 has been shown to form aggregates due to high concentrations of inorganic phosphate *in vitro* [31, 32]. Yet, the structural nature of the aggregation of DJ-1 *in vitro* and in the human brain, and its impact on the biochemical and biological functions of protein has not been elucidated.

In this study, we sought to characterize the structural and mechanistic processes underlying the aggregation of DJ-1 *in vitro* and the effects of aggregation on the protein's biochemical functions. Moreover, we examined a potential link between DJ-1 aggregation and the pathology of PD and AD in diseased and healthy post-mortem brain tissue.

Materials and Methods

Materials

DJ-1 was prepared as described below. For the DJ-1 expression experiments, we used chloramphenicol, carbenicillin, ampicilin antibiotics and *E.coli* bacteria purchased from Sigma Aldrich, isopropyl β-D-1-thiogalactopyranoside (IPTG) from ThermoFisher Scientific. Yeast extract and Tripton are products of Molar Chemicals Ltd. During DJ-1 purification we used Prescission Protease enzyme and L-glutathione ordered from Sigma Aldrich. The concentration of DJ-1 in experimental samples were determined by Bradford reagent (Sigma-Aldrich).

Bovine serum albumin (BSA, lyophilized powder, >98 %), ammonium persulfate (APS, 98 %), N,N,N',N'-tetramethylethylendiamine (TEMED, 99 %), acrylamide/ bis-acrylamide 30% w/w solution (BioReagent, suitable for electrophoresis), 1,4-dithiothreitol (DTT, 98%), hydrogen-peroxide 30% w/w solution (H_2O_2) and Thioflavin T (ThT, 98 %), were purchased from Sigma-Aldrich. Pentamer formyl thiophene acetic acid (pFTAA) was synthesized by the Molecular Imaging Chemistry Laboratory, University of Cambridge and followed the synthetic strategy described by Aslund and co-workers[33]. For the buffer solutions the tris-(hydroxylmethyl)-amino-methane hydrochloride (Tris-HCl, 99.8 %), potassium dihydrogen phosphate (analytical reagent (AR) grade level), disodium hydrogen phosphate 12-hydrate (AR grade level), potassium chloride (99.5%), sodium chloride (AR grade level) were purchased from Molar Chemicals. Disuccinimidyl suberate crosslinker (DSS) was bought from ThermoFisher Scientific. The water used for all reactions and solutions was MilliQ grade from a water purification facility (Millipore Milli-Q Gradient, $\kappa > 18.2$ Ωm). The pH values were adjusted by adding 1 M HCl or 1 M NaOH (Molar Chemicals).

DJ-1 expression and purification

Briefly, Rosetta (DE3) competent *E.coli* cells containing the full length human DJ-1 coding sequence between the NcoI and BamHI restriction sites of the pGEx expression vector (Novagen) were grown at 37°C in LB medium. (After cleaving the GST tag from the fused protein the remaining DJ-1 differs by an additional five amino acids (GPLGS – Precision Protease cleavage site residue and linker) from the native human DJ-1, which are present on the N-terminal of the protein.) LB medium was supplemented with chloramphenicol (25 mg/ml) and ampicillin (50 mg/ml) at 37°C. After reaching OD 0.8, overnight protein production was induced at 18°C by the addition of 0.1 mM IPTG (final concentration). On the next day, cells were centrifuged at 5,000 rpm for 10 minutes at 4°C using a Beckman centrifuge. The pellets were suspended with 100 mM PBS buffer at pH 7.4 and were then centrifuged again (at 4°C, 4000 rpm, 30 min). The resulting supernatants were discarded, and the residue suspended in lysis buffer (50 mM Tris-HCl, 100 mM NaCl, 1 mM EDTA, 0.1 % Igepal, 1 mM DTT at pH 7.4), then frozen at -80°C (without liquid nitrogen) until needed for protein purification.

For the purification of DJ-1, cells were thawed and lysed with intense sonication, then the collected lysates were centrifuged at 20,000 rpm for 30 minutes at 4°C. The supernatants were poured onto a pre-equilibrated GSTrap™ 4B column (GE Healthcare). Before elution the column was washed with the binding buffer (PBS, 1 mM DTT at pH 7.4), and then the protein was eluted using elution buffer (50 mM Tris-HCl, 20 mM reduced glutathione, 1 mM DTT at pH 8). After the elution, protein was dialyzed into 50 mM Tris-HCl, 100 mM NaCl, 1 mM EDTA and 0.5 mM DTT (pH 7.4) and Prescission Protease (1 µl enzyme to 5 mg protein) overnight at 4°C. Next day, dialysed protein was poured onto the GST column, pre-equilibrated with binding buffer, and collected flow through protein solution. The protein content of samples

was determined using the Bradford reagent at 595 nm with UV-Vis spectroscopy and purities were checked on a 12 % SDS-PAGE. DJ-1 samples stored at -80 °C.

Oxidation and over oxidation of DJ-1

DJ-1 (30 µM) was incubated with H_2O_2 in 10 or 100 fold excess to generate DJ-$1_{Cys106(SO2-)}$ and DJ-$1_{Cys106(SO3-)}$, respectively, at 4 °C in 20 mM phosphate buffer (pH 7.4) for 3 hours. Excess H_2O_2 was removed by dialysis against 20 mM phosphate and 10 mM NaCl buffer (pH 7.4) overnight. The oxidation status of all DJ-1 proteins was determined by LC-MS.

Liquid chromatography - mass spectrometry (LC-MS) of DJ-1

The molecular weights of the DJ-1 redox isoforms were confirmed using a Triple TOF 5600+ hybrid Quadrupole-TOF LC/MS/MS system (Sciex, Singapore, Woodlands) equipped with a DuoSpray IonSource coupled with a Shimadzu Prominence LC20 UFLC (Shimadzu, Japan) system consisting of binary pump and an autosampler. Data acquisition and processing were performed using Analyst TF software version 1.7.1 (AB Sciex Instruments, CA, USA). Chromatographic separation was achieved by Thermo Beta Basic C8 (50 mm × 2,1mm, 3 µm, 150 Å) HPLC column. Sample was eluted in gradient elution mode using solvent A (0.1% formic acid in water) and solvent B (0.1% formic acid in ACN). The initial condition was 20% B for 1 min, followed by a linear gradient to 90% B by 4 min, from 5 to 6 min 90% B was retained; and from 6 to 6.5 min back to initial condition with 20 % eluent B and retained from 6.5 to 9.0 min. Flow rate was set to 0.4 ml/min. The column temperature was 40 °C and the injection volume was 5 µl. Nitrogen was used as the nebulizer gas (GS1), heater gas (GS2), and curtain gas with the optimum values set at 30, 30 and 35 (arbitrary units), respectively. Data were

acquired in positive electrospray mode in the mass range of m/z=300 to 2500, with 1 s accumulation time. The source temperature was 350 °C and the spray voltage was set to 5500 V. Declustering potential value was set to 80 V. Peak View SoftwareTM V.2.2 (version 2.2, Sciex, Redwood City, CA, USA) was used for deconvoluting the raw electrospray data to obtain the neutral molecular masses. In the non-oxidized ("reduced") DJ-1$_{Cys106(S-)}$ sample the ratio of DJ-1 C106 thiol (-SH) to sulfinic acid (-SO_2H) was calculated to be 85 to 15. In the DJ-1$_{Cys106(SO2-)}$ sample the ratio of DJ-1 C106 sulfinic acid (-SO_2H) to sulfonic acid (-SO_3H) was calculated to be 83 to 17. In the DJ-1$_{Cys106(SO3-)}$ sample the ratio of DJ-1 C106 in sulfinic acid (-SO_2H) to sulfonic acid (-SO_3H) form was calculated to be 13 to 87. The resolution of the mass spectrometer was above 30000 full width at half maximum over the entire mass range enabling the deconvolution of the multiply charged ion series to zero charge state with accuracy of less than 1 Da. The total ion chromatogram**,** mass spectra and deconvoluted masses are shown in Fig. S1.

DJ-1 aggregation experiments

DJ-1$_{Cys106(S-)}$, DJ-1$_{Cys106(SO2-)}$ and DJ-1$_{Cys106(SO3-)}$ samples were incubated under quiescent conditions without shaking at 30 μM protein concentrations at 37 °C, pH 7.4 in 20 mM phosphate, 5 mM NaCl buffer. Only in the case of the FTIR and DJ-1 glyoxalase experiments were the DJ-1 samples incubated at 60 μM.

Dynamic light scattering (DLS) measurements

Measurements were taken at 25 °C using a Malvern Zetasizer Nano ZS instrument equipped with a thermostat cell. DJ-1 in 20 mM phosphate, 10 mM NaCl (pH 7.4) buffer at concentrations of

30 μM was centrifuged at 10,000 rpm for 45 min at 4 °C. The samples were filtered through a 0.22 μm filter before the measurements. 100 μl of the supernatants were added to the cuvette, and the light scattering intensity was collected 30 times at an angle of 90° using a 10 sec acquisition time. The correlation data was exported and analyzed using the nanoDTS software (Malvern Instruments). The samples were measured at 60 min and thereafter at in 24 hour intervals. In each case three parallel measurements were taken. Data was averaged and plotted as a function of time, then fitted to a saturation curve using Origin 8 software.

Determining the concentration of DJ-1 aggregates

We followed the aggregation rate of DJ-1 protein as a function of time. DJ-$1_{Cys106(S-)}$, DJ-$1_{Cys106(SO2-)}$ and DJ-$1_{Cys106(SO3-)}$ samples were incubated at 37 °C, for 2 weeks at 30 μM in 20 mM phosphate, 5 mM NaCl buffer. The aggregate rich phase and the monomer rich phase in the samples were separated with an ultracentrifugation technique (v = 100,000 g for 2 hours), thereafter the protein concentration was determined using the Bradford reagent. Soluble DJ-1 concentrations were plotted as a function of time.

Far UV circular dichroism spectroscopy (CD)

DJ-$1_{Cys106(S-)}$, DJ-$1_{Cys106(SO2-)}$ and DJ-$1_{Cys106(SO3-)}$ samples were incubated at 37 °C in 20 mM phosphate, 5 mM NaCl buffer under quiescent conditions at pH 7.4 for 5 days. CD measurements were done on the incubated samples at the start of the incubation and 5 days later diluted to 10 μM in 20 mM phosphate, 5 mM NaCl buffer at pH 7.4. The aggregate rich phase was separated from the monomer rich phase with an ultracentrifugation technique (v = 100,000 g for 2 hours). CD spectra were recorded using JASCO J-720 spectrometer. The final spectrum was taken as a background-corrected average of 5 scans carried out under the following

conditions: wavelength range 250–190 nm at 25 °C; bandwidth was 1 nm; acquisition time was 1 sec and intervals were 0.2 nm. Measurements were performed in a 0.01 cm cell. CD spectra were plotted in mean residue molar ellipticity units (deg cm^2 $dmol^{-1}$) calculated by the following equation: $[\Theta] = \Theta_{obs}/(10ncl)$ where $[\Theta]$ is the mean residue molar ellipticity as a function of wavelength, Θ_{obs} is the measured ellipticity as a function of wavelength (nm), *n* is the number of residues in the protein, *c* is the concentration of the protein (M), and *l* is the optical path length (cm). Secondary structural analysis of DJ-1 using CD spectroscopic data was carried out using the BeStSel (Beta Structure Selection) software[35].

Fourier transform infrared spectroscopy (FTIR) spectroscopy

FTIR spectra were acquired for DJ-$1_{Cys106(S-)}$, DJ-$1_{Cys106(SO2-)}$ and DJ-$1_{Cys106(SO3-)}$ at the start of incubation and 5 days later using Varian 2000 FTIR spectrometer, equipped with a sensitive liquid N_2 cooled MCT detector. The incubations of the DJ-1 and BSA samples were in 20 mM phosphate, 10 mM NaCl buffer, at pH 7.4 under quiescent conditions, at 60 µM protein concentration. Fourier-transformed background-corrected absorption spectra were taken at 25 °C between 1,000 and 4,000 cm^{-1} as an average of 64 scans, acquired at a resolution of 2 cm^{-1} and an optical aperture of 0.5 cm. All spectra were post-processed using the Thermo Galactic GRAMS/AI™ Spectroscopy Software 7.02. An atmospheric correction algorithm was used to remove any water vapour bands from the final absorption spectra. Spectra were zeroed between 1,400 and 1,800 cm^{-1}, and the 2nd derivative spectra calculated.

Transmission electron microscopy (TEM) measurements

TEM was used to estimate the size and structural morphology of DJ-$1_{Cys106(S-)}$, DJ-$1_{Cys106(SO2-)}$ and DJ-$1_{Cys106(SO3-)}$ incubated for 5 days in 20 mM phosphate, 10 mM NaCl buffer, at pH 7.4 at

30 μM protein concentration under quiescent conditions. Protein samples were deposited on the Formvar-coated 300 mesh copper grids and negatively stained with 1 % (w/v) aqueous uranyl acetate. Grids were then rinsed with water to remove salts and urea. Samples were examined on a MORGAGNI 268D transmission electron microscope operated at 100 kV.

Fibril formation, Thioflavin T (ThT) and pFTAA fluorescence assay

Protein aggregate formation was monitored using ThT and pFTAA assays. The enhanced fluorescence of the dye ThT and pFTAA on binding to fibrils or β-sheet structured protein aggregates was recorded. DJ-1$_{Cys106(S-)}$, DJ-1$_{Cys106(SO2-)}$ and DJ-1$_{Cys106(SO3-)}$ and BSA samples were incubated at 30 μM concentration in 20 mM phosphate, 10 mM NaCl (pH 7.4) at 37 °C under quiescent conditions. For the ThT and pFTAA assays, aliquots of 10 μl protein solutions were removed and diluted to 1000 μl solutions with 5 μM ThT and pFTAA, respectively, in 20 mM phosphate buffer and 5 mM NaCl (pH 7.4). The fluorescence intensity and protein assembly formation was recorded at 490 nm with excitation at 450 nm for ThioT, and 520 nm with excitation at 450 nm for pFTAA using a Fluoromax-3 spectrometer. The cuvette was incubated at 25 °C. Data were averaged and plotted as a function of time, then fitted to a sigmoidal curve using Origin 8 software.

Native PAGE electrophoresis

DJ-1$_{Cys106(S-)}$, DJ-1$_{Cys106(SO2-)}$ and DJ-1$_{Cys106(SO3-)}$ samples were incubated at 30 μM concentration in 20 mM phosphate, 10 mM NaCl (pH 7.4) at 37 °C under quiescent conditions. Samples of DJ-1 for Native PAGE electrophoresis were applied without any treatment at the start of the incubation and after 24 hours. DJ-1 proteins are prepared in a non-reducing non-denaturing sample buffer, which maintains the proteins secondary structure and native charge density.

Native PAGE was performed with a Cleaver Scientific Ltd. electrophoresis system. For a Native PAGE stacking gel we used a 0.375 M Tris-HCl, pH 8.8, and AAm / BAAm 30 % w/v solution with 10 % AAm percentage. The sample buffer contained 62.5 mM Tris-HCl pH 6.8, 25 % glycerol and 1 % Bromphenol Blue. The gel was run using 25 mM Tris-HCl with a 192 mM glycine running buffer at pH 8.3 for 90 min at 150 V and 20-30 mA. The gel was stained with Coomassie Blue R250. We used disuccinimidyl substrate (DSS) crosslinked non-aggregated DJ-1 as a marker on Native PAGE, because the DSS can stabilize the dimer form of DJ-1. During the protocol we prepared 50 mM solutions of DSS by dissolving 10 mg DSS in 540 μL of dry DMSO. Using a 20-fold excess approach (20:1 Crosslinker:Protein), we added the crosslinker solution to the DJ-1 sample in 25 mM phosphate buffer at pH 7.4. The sample was allowed to react at 4 °C for 2 hours, after which any unreacted DSS was quenched with 50 mM Tris-HCl buffer at pH 7.4 and allowed to react for 15 minutes at room temperature.

Western Blot

After Native PAGE separation of DJ-1 samples, they were transferred to a prevetted (in 100% methanol) Immobilon-P Transfer Membrane (Millipore) for Western blot analysis. Protein transfer was performed with Trans-Blot® Turbo™ Blotting System (Bio-Rad). After transfer, membranes were blocked with blocking buffer containing 5% milk powder dissolved in Tris-buffered saline (TBS; pH 7.6) overnight at 4°C. Blocked membranes were incubated with mouse anti-oxDJ-1 antibody (mAb) (clone M149, Millipore), $mAb_{anti\text{-}oxDJ\text{-}1}$, dissolved in blocking buffer at room temperature (RT) for 1 hour. After that membranes were washed 3 times with TBS containing 0,1% Tween 20 (TBST), and incubated with HRP-conjugated anti-mouse secondary mAb (Jackson Immunoresearch) dissolved in blocking buffer, for 1 hour at RT. After incubation,

membranes were washed 3 times with TBST and developed using the enhanced chemiluminescence reagent, and blue sensitive Super RX-N Fuji Medical X-RAY films.

Anti-oxidized DJ-1 antibody validation with HAP1 DJ-1 knock-out (KO) cell line

Confluent SH-SY5Y (ATCC), HAP1 and HAP1 DJ-1 KO (Horizon) cells were lysed in Cell Extraction Buffer PTR 5X (Abcam, ab193970) and equal amounts of protein were separated in 12% SDS-PAGE and transferred to PVDF membrane. The membrane was blocked with 5% (w/v) nonfat dry milk in TBS buffer containing 0.1% Tween 20 for an hour. Immunoblot was performed with anti-DJ1 antibody (ENZO 1:2000), $mAb_{anti\text{-}DJ\text{-}1}$, and anti-oxDJ-1 antibody (clone M149, Millipore, 1:1000), $mAb_{anti\text{-}oxDJ\text{-}1}$. Tubulin (Sigma 1:10 000) was used as loading control. SH-SY5Y, HAP1 and HAP1 DJ-1 KO cells were lysed at the confluent stage and after protein content normalization, the samples were boiled in Lemmly puffer and then an immunoblot was performed.

DJ-1 Glyoxalase Activity Assay

Preparation of aggregated DJ-1 for glyoxalase activity assay was done in the following way. DJ-$1_{Cys106(S\text{-})}$, samples were incubated at 30 μM concentration in 20 mM phosphate, 10 mM NaCl (pH 7.4) at 37 °C for 5 days under quiescent conditions. Starting protein samples were ultracentrifuged at 54,000 rpm for 60 min at 4 °C for glyoxalase assay, while DJ-$1_{Cys106(S\text{-})}$ samples incubated for 5 days were applied without ultracentrifugation. The methylglyoxal (MGO) depletion assay was optimized for plate based usage in-house and applied as follows: a 200 μL DNPH reagent mixture (composed of 10V/V% DMSO 8V/V% 36 m/m% HCl, and 400 μM DNPH (dinitrophenylhydrazine) in MQ water) was mixed with a 15μL sample with or without DJ-1 samples and with 0.85 mM MGO initial concentration, incubated for at least 5

minutes at room temperature (rt) than visualized with 20m/m% NaOH solution. Absorbance at 560 nm was measured within *1-7* min following the sodium-hydroxide addition. Calibration was done and fitted with a quadratic function. DJ-1$_{Cys106(S-)}$ samples ((1) initial, (2) incubated for 5 days (aggregated), and (3) initial reacted with IAA (inhibited)) were prepared in triplicate in qPCR plate (ThermoScientific) and the 15µL samples were taken within one hour. Linears were fitted to the corresponding time dependent MGO concentrations and the mean and standard deviation of the initial velocities-slopes were plotted in the bar charts as the activity data. IAA was added to give a final concentration of 0.9 mM in a negligable volume (<1% of total) and incubated at rt for 20min before MGO Assay initiation. The DTT concentration was 350 µM in all samples incubated. MGO (as 40m/m% aqueous solution), DNPH, plates (Greiner 96 well plates, polystyrene non-sterile) were purchased from Sigma, Hungary while MQ water was prepared in-house using the appropriate equipment and sodium-hydroxide was purchased from Molar Chemicals Kft, Hungary.

Clinical Samples

Human post mortem brain tissue included formalin-fixed paraffin embedded sections of amygdala (10 µm thickness) from 5 PD cases and 4 age-matched controls without known neurological disease. PD cases had a mean (SD) age of 81.9 (7.7) years at death and controls were 79 (7.6) years old. PD disease duration was 6.6 - 23.9 years. In addition, frozen sections (~25µm thickness) of human post mortem brain tissue from the frontal cortex (BA9) of 2 AD cases and 2 controls were investigated. The AD cases were 83 and 78 years old at death, modified Braak tau stage 5 and 4, and disease duration 10 and 5 years, respectively. The controls were aged 74 and 69 at death.

Triple-labeling immunofluorescence

Post-mortem brain slices were placed in xylene overnight and rehydrated with decreasing level of ethanol, before being left in sodium citrate buffer (0.05% Tween20, pH 6.0) for 20min at 60°C. After blocking with 0.3% Triton X-100 and 5% serum for 1hr, slides were incubated overnight with various primary antibodies including Anti-(Cys106) oxDJ-1 (Millipore MABN1773, 1:250), $mAb_{anti\text{-}oxDJ\text{-}1}$, phosphorylated (Ser129) α-synuclein (Abcam ab51253, 1:500), $mAb_{p\text{-}\alpha syn}$, phospho-(Thr205) Tau (Covance SIG-39448, 1:500), $mAb_{p\text{-}Tau}$, amyloid-Beta (Abcam, ab2539, 1:500), $mAb_{A\beta}$, and the pentameric formyl thiophene acetic acid pFTAA (3μM). Slides were then stained with secondary antibodies (Alexa 405 and Alexa 647, Molecular Probes, 1:1000), differentiated for 3min in escalating levels of ethanol, and blocked with 0.2% Sudan black B (Sigma) in 70% ethanol for 30sec, before visualization using a TCS SP2 confocal microscope (Leica). Quantification of signal intensity and colocalization were performed using Leica LAS 2.6.0. Statistical analysis was performed using multivariate ANOVA with *post-hoc* Bonferroni correction to adjust for multiple comparison, using SPSS release 25.0.0.

Data availability

The datasets generated during the current study are available from the corresponding author on request.

Results

DJ-1 aggregates into β-sheet structured soluble aggregate and fibrillar aggregates *in vitro* under physiological conditions. We examined the propensity of DJ-1, in various oxidation states of Cys106, to aggregate into low molecular weight aggregate. This was done using dynamic light scattering (DLS) under physiologically relevant conditions using phosphate and Tris buffers. Previously we have determined that the hydrodynamic diameter (D_h) of the DJ-1 homodimer in both its native and various oxidized Cys106 states is almost identical under physiological conditions [34]. In our new experiments, DJ-1 formed DLS detectable aggregate in both buffers within hours when homodimeric DJ-1 was incubated in quiescent conditions at 30 μM, 37^{o}C and pH 7.4 (Fig 1.) in both phosphate and Tris buffers. DJ-1 when oxidized at residue Cys106 (sulfinate, DJ-1$_{Cys106(SO2-)}$, and sulfonate, DJ-1$_{Cys106(SO3-)}$) formed aggregate significantly faster with larger D_h compared to DJ-1 in the Cys106 thiolate state (DJ-1$_{Cys106(S-)}$), while BSA did not lead to the formation of detectable aggregate (Fig. 1a-c, Table S1.). In the case of DJ-1$_{Cys106(S-)}$, aggregate appeared after 5 and 8 hours in phosphate and Tris buffer, respectively, while the oxidized DJ-1 samples formed aggregate as early as 1 hour irrespective of their buffer solutions. This aggregation of DJ-1 was then further investigated by measuring the concentration of homodimeric DJ-1 during the aggregation experiments, performed in quiescent conditions at 30 μM, 37^{o}C and pH 7.4, in phosphate buffer, by separating homodimeric and aggregated DJ-1 using ultracentrifugation. After ultracentrifugation of incubated DJ-1 samples, the protein in the supernatant was observed to be in a homodimeric state based on its observed D_h size (5.66 nm ± 0.83), similar that seen in the starting sample, while the pellet contained aggregated DJ-1 (Fig. S2.). In the samples of DJ-1$_{Cys106(SO2-)}$ and DJ-1$_{Cys106(SO3-)}$ the extent of concentration decrease of homodimeric DJ-1 was higher in the supernatant and hence aggregate formation was faster compared to DJ-1$_{Cys106(S-)}$. Overall, the aggregation process of all DJ-1

samples tested saturated after about 12 days in the assay with 30 to 50 % of the protein samples being in an aggregated state at this time point.

Next, the aggregation of DJ-1 was monitored using the fluorescence intensity of Thioflavin T (ThT) and of pentameric formyl thiophene acetic acid pFTAA (Fig. 1 d and e), dyes whose fluorescence increases when they bind to polypeptides with extended β-sheet structures (such as amyloid). The fluorescence intensity of ThT and pFTAA significantly increased during the incubation of the DJ-1 samples demonstrating the formation of β-sheet structures during the aggregation of DJ-1.

We then sought to investigate whether the DJ-1 aggregates had an intrinsic fluorescence signature characteristic of cross-β sheeted scaffold polypeptides[36] such as amyloid. While no well-defined fluorescence peak was observed, the fluorescence intensity of DJ-1 between 445-485 nm during its aggregation (in quiescent conditions at 30 μM, 37°C and pH 7.4 for 5 days in phosphate buffer) also resembled a macroscopic aggregation curve with a short lag phase (Fig. 1f), which had a similar evolution for all three of the DJ-1 Cys106 states we investigated, although samples of DJ-1$_{Cys106(SO2-)}$ and DJ-1$_{Cys106(SO3-)}$ generated higher fluorescence intensities compared to DJ-1$_{Cys106(S-)}$.

We next investigated the morphology of solid DJ-1 aggregates (Fig. 1 g-i) formed, when incubating homodimeric DJ-1 under quiescent conditions for 5 using transmission electron microscopy (TEM). We found that the morphology of aggregates was dependent on the oxidation state of the DJ-1 Cys106 residue. DJ-1$_{Cys106(S-)}$ formed a mixture of amorphous aggregates with some filamentous assemblies, while DJ-1$_{Cys106(SO2-)}$ and DJ-1$_{Cys106(SO3-)}$ formed more fibril-like aggregates.

The aggregates of DJ-1 generated during the aggregation experiments were found to contain substantially higher amounts of β-sheet structures compared to the native homodimeric protein.

After 5 days of incubation of DJ-1 (using all three Cys106 states) under quiescent conditions the homodimeric and aggregated forms of DJ-1 were separated by ultracentrifugation and the pellet containing aggregated DJ-1 was diluted in phosphate buffer. From this, the secondary structure content of DJ-1 in the supernatant and pellet was determined by circular dichroism (CD). For all the pellet samples of DJ-1 the intensity of the minima at 208 nm decreased and the minima at 222 nm shifted toward 225 - 226 nm (Fig. 2 a-c), while for the supernatant no significant changes were observed compared to the initial homodimeric structural state of DJ-1. BSA was used as a control (Fig. 2g), and this showed no secondary structural changes compared to the starting sample. The proportion of the structural elements from all the supernatant samples was calculated using BeStSel[35] and found to be: 50.9-67.0-% α-helix and 24.7 – 40.9 % β-sheet. This matches well with the structural composition of starting DJ-1 samples indicating that homodimeric DJ-1 is the main component of this fraction, while the samples originating from the pellet had a decrease in α-helical structures to 6.8-8.9 % with a corresponding increase in β-sheet structure to be 70. 5 – 79.3 % (Table 1). Analogous results were found for native and oxidized states of DJ-1.

These observations were further supported by the second derivative spectra from Fourier transform infrared spectroscopy (FTIR) studies, in which starting samples of native and oxidized DJ-1 in the Amide I band region had a minimum at around 1650 cm^{-1} (indicating α-helical content) and another at around 1630 cm^{-1} (indicating β-sheet content). After incubation of DJ-1 for 5 days under quiescent conditions, the intensity of the second derivative bands around 1650 cm^{-1} decreased, while the ones around 1630 cm^{-1} substantially increased with a shift to lower wavenumbers suggesting the formation of intermolecular hydrogen bonds between β-sheets. All this suggests that the β-sheet content of the protein significantly increased at the expense of α-helical content. BSA was used as control (Fig. 2h) and showed no secondary

structural changes even after 5 days of incubation. Overall, we found that our starting samples containing native homodimeric DJ-1 transitioned into soluble aggregates that had a high parallel and antiparallel β-sheet structural content. Similar transitions from a native to high content β-sheet structure has previously been observed using CD and FTIR with pathological amyloid forming proteins, such as α-synuclein[37].

The aggregation of DJ-1 results in loss of its glyoxalase function. The effect of aggregation of DJ-1 on its glyoxalase activity[19] was investigated next. In an MGO depletion assay (Fig. 3a) the glyoxalase activity of DJ-1$_{Cys106(S-)}$, incubated for 5 days under quiescent conditions, decreased to approximately half of the activity observed for native dimeric DJ-1$_{Cys106(S-)}$. In addition, this activity was almost completely lost for DJ-1$_{Cys106(S-)}$ when it was inactivated by iodoacetamide (IAA), a strong alkylating agent of thiols. The extent of this loss of glyoxalase activity for aggregated DJ-1$_{Cys106(S-)}$ was proportional to the degree of aggregation observed for DJ-1 (Fig. 1c), suggesting that structural changes in DJ-1 due to the aggregation of the protein led to the impairment of its glyoxalase function.

The aggregation of DJ-1 may happen through the loss of its homodimeric structure. The aggregation of DJ-1 was also monitored using Native PAGE, which showed that native and oxidized states of DJ-1 were composed of a stronger band, representing DJ-1 homodimers, and a weaker band, representing monomeric DJ-1 (Fig 3b). As a marker for homodimeric DJ-1$_{Cys106(S-)}$ disuccinimidyl suberate (DSS) was used to covalently link homodimeric DJ-1 and stabilize its dimeric structure. The cross-linked DJ-1 ran on the Native PAGE in exactly the same pattern as that seen for the native homodimeric DJ-1 samples. While aggregated DJ-1, sampled after 72 hours of incubation of homodimeric DJ-1, consisted of bands representing high molecular weight

complexes of DJ-1 and monomeric DJ-1, a band representing homodimeric DJ-1 was not detected. We then went on to perform Native PAGE western blots using an oxidized DJ-1 specific antibody, $mAb_{anti\text{-}oxDJ\text{-}1}$, and observed that it recognizes DJ-$1_{Cys106(SO2\text{-})}$ and DJ-$1_{Cys106(SO3\text{-})}$ specifically as well as both homodimeric and high molecular weight complexes of DJ-1 (Fig. 3c).

Oxidized DJ-1 aggregates can co-localize with Lewy bodies, neurofibrillary tangles and amyloid plaques in human PD and AD patients' post-mortem brain tissue. DJ-1 aggregation was also investigated in healthy and diseased human post-mortem brain tissues. Triple-labeling immunofluorescence studies (TIF) were performed, which showed that the $mAb_{anti\text{-}oxDJ\text{-}1}$ strongly immunolabeled post-mortem PD (n=5) and AD (n=4) patient tissue from the amygdala and frontal cortex, respectively, suggesting that significant amounts of DJ-$1_{Cys106(SO2\text{-})}$ and DJ-$1_{Cys106(SO3\text{-})}$ (oxidized-DJ-1) exist in the diseased brain, while clearly less labelling was observed in healthy brain samples. The DJ-1 specificity of the $mAb_{anti\text{-}oxDJ\text{-}1}$ was further validated by showing that $mAb_{anti\text{-}oxDJ\text{-}1}$ detected DJ-1 under oxidative stress conditions in HAP1 cells by western blot, while it did not detect DJ-1 in HAP1 DJ-1 knock-out cells (Fig. S4.). These results suggest that oxidized DJ-1 levels are increased in PD and AD brain tissue compared to healthy control. Moreover, in the PD brain, $mAb_{anti\text{-}oxDJ\text{-}1}$ labeling co-localized with pFTAA fluorescence (Fig. 4a) demonstrating that oxidized DJ-1 was mostly observed in areas where proteins with β-sheet rich structures, such as amyloid fibrils are found. In contrast, in healthy brain tissue minimal pFTAA fluorescence was detected. It was also observed that $mAb_{anti\text{-}oxDJ\text{-}1}$ staining co-localized with anti-phospho (at Ser129) α-synuclein mAb ($mAb_{p\text{-}\alpha syn}$) labeling (Fig. 4b), all of which suggests that oxidized DJ-1 is a component of Lewy bodies. Next, we showed that $mAb_{anti\text{-}oxDJ\text{-}1}$ staining co-localized with anti-phospho (at Ser205) Tau mAb ($mAb_{p\text{-}Tau}$) labeling

and pFTAA fluorescence (Fig. 4c), again implying that oxidized DJ-1 can be associated with Tau neurofibrillary tangles (NFTs) in the PD brain. Similarly, TIF showed that $mAb_{anti\text{-}oxDJ\text{-}1}$ labelling distinctly associated with anti-$A\beta_{1\text{-}42}$ amyloid mAb ($mAb_{A\beta}$) (Fig. 4d), and anti-Tau mAb_{Thr205} staining (Fig. 4e) and pFTAA fluorescence in the post-mortem AD brain tissue. Again, there was minimal $mAb_{anti\text{-}oxDJ\text{-}1}$ staining seen in healthy brain tissue, suggesting that oxidized DJ-1 is once more associated with amyloid plaques and neurofibrillary tangles (NFTs) in the AD brain. A semiquantitative fluorescence signal intensity analysis confirmed that the levels of both $mAb_{anti\text{-}oxDJ\text{-}1}$ staining and pFTAA levels are both significantly higher in PD and AD post-mortem brains, as compared to healthy subjects (Fig. 4f). $mAb_{anti\text{-}oxDJ\text{-}1}$ staining colocalizing with pFTAA fluorescence was also significantly increased in PD and AD post-mortem brains (Fig. 4g), showing the upregulation of oxidized DJ-1 aggregation in PD and AD patients.

Discussion

Our results demonstrate, for the first time, that DJ-1 aggregates into β-sheet structured soluble aggregates *in vitro* under physiological conditions and that this process may be enhanced by the oxidation of its catalytic Cys106 residue. The aggregation of DJ-1 was observed *in vitro* under physiologically relevant conditions using either phosphate or Tris buffers, suggesting that the aggregation of the protein can happen without the presence of inorganic phosphate.

The pathological evidence for this was confirmed by showing that aggregated oxidized DJ-1 exists in the post mortem brains of patients with PD or AD. Previous reports have shown that DJ-1 co-localizes with α-synuclein fibrils in Lewy bodies[39, 40], or with NFTs[41] and that the DJ-1 protein is present in amyloid plaques from AD patients[42]. Moreover, two other studies have shown that DJ-1 levels in the detergent-insoluble fractions of post-mortem brain tissue from

the cingulate cortex of patients with idiopathic PD with Dementia with Lewy bodies[43] or the cerebellar white matter in patients with multiple system atrophy (MSA)[39] were dramatically increased compared to aged matched healthy controls. These previous reports provide strong evidence for the existence of insoluble DJ-1 and soluble DJ-1 aggregates in brain tissue of patients with PD and Dementia with Lewy bodies as well as AD and MSA, which suggests that DJ-1 may be self-aggregating and/or aggregating with other proteins, such as α-synuclein, tau and Aβ42, to form β-sheet structured aggregate and amyloid aggregates in the brain in these diseases.

We have also now shown for the first time that the aggregation of DJ-1 leads to the loss of one of its key enzymatic functions, its glyoxalase activity, through a complete loss of its active homodimeric state. It is likely that DJ-1 aggregation would also result in the loss of its other enzymatic functions and in its ability to regulate redox and protein homeostasis [7]. These findings suggest that DJ-1 aggregation results in the loss of DJ-1 function, which could contribute to disease onset and progression.

We have observed that $mAb_{anti\text{-}oxDJ\text{-}1}$ strongly immunolabeled post-mortem PD and AD brain tissue while less labelling was observed in control healthy brain samples. These results are in line with two previous studies, which report that oxidized DJ-1 levels are increased in PD[40] and AD[10] brain tissue compared to healthy ones.

The loss of wild type DJ-1 function due to the loss of native structure of the protein and its aggregation parallels the effects of some specific mutations (L166P, L10P, and ΔP158) in the DJ-1 encoding gene, PARK7, that cause familial autosomal recessive early-onset PD. These mutations in DJ-1 cause structural instability in its native tertiary homodimeric structure which means that the protein loses its ability to homodimerize and this in turn may lead to the aggregation of these mutant DJ-1 proteins[44]. For instance, the L166P DJ-1 mutant was

observed mostly in soluble high molecular weight complexes and not as a homodimer in cell lysates[45], while the **Δ**P158 and L10P DJ-1 mutants were observed in cells to form inclusions [46].

Conclusion

Our results demonstrate that DJ-1 can form β-sheet structured soluble DJ-1 aggregate and fibrillar aggregates and that specific oxidation of the protein at Cys106 promotes this process. These aggregated forms of DJ-1 were found to exist pathologically in the post-mortem brains of patients who had died with PD or AD. Moreover, it was observed that the loss of function of DJ-1, such as its glyoxalase activity, and conceivably its ability to regulate redox and protein homeostasis[7], due to its aggregation could contribute to the onset and progression of these diseases. All of this implies that DJ-1 may be a critical central player in the development of proteinopathies in different neurodegenerative disorders, and thus any drug discovery approach that aims to stabilize the native functional homodimeric structure of DJ-1 to reduce its aggregation could have wide ranging therapeutic implications.

List of Abbreviations

AD: Alzheimer's disease; PD: Parkinson's disease; AR: analytical reagent; IPTG: isopropyl β-D-1-thiogalactopyranoside; BSA: bovine serum albumin; APS: ammonium persulfate; TEMED: N,N,N',N'-tetramethylethylendiamine; DTT: 1,4-dithiothreitol; H_2O_2: hydrogen-peroxide, ThT: Thioflavin T; pFTAA: pentamer formyl thiophene acetic acid; Tris-HCl : tris-(hydroxylmethyl)-amino-methane hydrochloride; DSS: disuccinimidyl suberate; DJ-

1$_{Cys106(S-)}$: DJ-1 in the Cys106 thiolate state; DJ-1$_{Cys106(SO2-)}$: DJ-1 oxidized at residue Cys106 in sulfonite state; DJ-1$_{Cys106(SO3-)}$: DJ-1 oxidized at residue Cys106 in sulfonate state. LC-MS: liquid chromatography - mass spectrometry; BeStSel: Beta Structure Selection; FTIR: fourier transform infrared spectroscopy; TEM: transmission electron microscopy; CD: circular dichroism spectroscopy; mAb: antibody; KO: knock-out; DNPH: dinitrophenylhydrazine; MGO: methylglyoxal; rt: room temperature; TIF: triple-labeling immunofluorescence; mAb$_{anti-DJ-1}$: anti-DJ1 antibody; mAb$_{anti-oxDJ-1}$: anti-(Cys106) oxDJ-1 antibody; mAb$_{p-\square syn}$: phosphorylated (Ser129) α-synuclein antibody; mAb$_{p-Tau}$: phospho-(Thr205) Tau antibody; mAb$_{\square\square}$: amyloid-Beta antibody; MSA: multiple system atrophy;

Declarations

Acknowledgements

The authors thank the Queen Square Brain Bank for Neurological Disorders for the PD and aged-matched control post mortem brain samples, the Cambridge Brain Bank (UK) for the AD post-mortem brain samples, and Brains for Dementia Research King's College London UK for aged-matched control post mortem brain samples used in the study for AD cases. The authors thank Dr. Czajlik and B. Czebe for their support with the *in vitro* aggregation experiments, Dr. R. Vuono and Dr. D. Williamson for their support of the TIF studies, Dr. O. Tietz for synthesizing and providing pFTAA.

Author's contribution

G.T. conceived the study, co-designed research experiments. K.S. performed all the *in vitro* DJ-1 aggregation experiments. T. I. and R. K. performed LC-MS experiments. W. K. designed and performed all fluorescence microscopy experiments. B.F. performed DJ-1 glyoxalase experiments. G.K. generated recombinant DJ-1 and co-performed *in vitro* DJ-1 western blot experiments. M.K., E.M. and A.M. co-performed DJ-1 western blot experiments. J.M. and Z.V. designed and performed the FTIR experiments. Y.Z. and C.W-G. supported fluorescence microscopy experiments. F.I.A., B.H., J.C.R. and R.A.B. and all other authors contributed to the analyses of the data and to the writing of the manuscript. All authors read and approved the final manuscript.

Funding

G.T. thanks the Hungarian Brain Research Program (2017-1.2.1-NKP-2017-00002) for funding and the NIHR Cambridge Biomedical Research Centre and Unit in Dementia (UK) for salary

support for Y. Z. R.A.B. and C.H.W.G. are supported by the NIHR Cambridge Biomedical Research Centre. R. A. B. is supported by the Wellcome Trust - Medical Research Council Cambridge Stem Cell Institute and is an NIHR Senior Investigator.

Competing interests

We have read the journal's policy and make the following statements on competing financial interests: some of the authors are employees and/or shareholders of Cantabio Pharmaceuticals as designated by Cantabio affiliation. This does not alter our adherence to all the journal's policies on sharing data and materials.

Ethics approval and consent to participate

All ethical approvals have been obtained as well as consent to participate.

Availability of data and material

All data generated and analyzed during the study are available from the corresponding author on reasonable request.

Consent for publication

All authors have consented for publication.

Supplementary Information

Fig. S1. – S4., Table S1

References

1. Riek R, Eisenberg DS: **The activities of amyloids from a structural perspective.** *Nature* 2016, **539:**227-235.
2. Sipe JD, Benson MD, Buxbaum JN, Ikeda SI, Merlini G, Saraiva MJ, Westermark P: **Amyloid fibril proteins and amyloidosis: chemical identification and clinical classification International Society of Amyloidosis 2016 Nomenclature Guidelines.** *Amyloid* 2016, **23:**209-213.
3. Glenner GG, Wong CW: **Alzheimer's disease: initial report of the purification and characterization of a novel cerebrovascular amyloid protein.** *Biochem Biophys Res Commun* 1984, **120:**885-890.
4. Lee VM, Goedert M, Trojanowski JQ: **Neurodegenerative tauopathies.** *Annu Rev Neurosci* 2001, **24:**1121-1159.
5. Selkoe DJ, Hardy J: **The amyloid hypothesis of Alzheimer's disease at 25 years.** *EMBO Mol Med* 2016, **8:**595-608.
6. Spillantini MG, Schmidt ML, Lee VM, Trojanowski JQ, Jakes R, Goedert M: **Alpha-synuclein in Lewy bodies.** *Nature* 1997, **388:**839-840.
7. Ariga H, Takahashi-Niki K, Kato I, Maita H, Niki T, Iguchi-Ariga SM: **Neuroprotective function of DJ-1 in Parkinson's disease.** *Oxidative medicine and cellular longevity* 2013, **2013:**683920.
8. Bonifati V, Rizzu P, van Baren MJ, Schaap O, Breedveld GJ, Krieger E, Dekker MC, Squitieri F, Ibanez P, Joosse M, et al: **Mutations in the DJ-1 gene associated with autosomal recessive early-onset parkinsonism.** *Science* 2003, **299:**256-259.

9. Taipa R, Pereira C, Reis I, Alonso I, Bastos-Lima A, Melo-Pires M, Magalhaes M: **DJ-1 linked parkinsonism (PARK7) is associated with Lewy body pathology.** *Brain* 2016, **139:**1680-1687.

10. Choi J, Sullards MC, Olzmann JA, Rees HD, Weintraub ST, Bostwick DE, Gearing M, Levey AI, Chin LS, Li L: **Oxidative damage of DJ-1 is linked to sporadic Parkinson and Alzheimer diseases.** *J Biol Chem* 2006, **281:**10816-10824.

11. Kahle PJ, Waak J, Gasser T: **DJ-1 and prevention of oxidative stress in Parkinson's disease and other age-related disorders.** *Free radical biology & medicine* 2009, **47:**1354-1361.

12. Aleyasin H, Rousseaux MW, Phillips M, Kim RH, Bland RJ, Callaghan S, Slack RS, During MJ, Mak TW, Park DS: **The Parkinson's disease gene DJ-1 is also a key regulator of stroke-induced damage.** *Proceedings of the National Academy of Sciences of the United States of America* 2007, **104:**18748-18753.

13. Inberg A, Linial M: **Protection of pancreatic beta-cells from various stress conditions is mediated by DJ-1.** *J Biol Chem* 2010, **285:**25686-25698.

14. Jain D, Jain R, Eberhard D, Eglinger J, Bugliani M, Piemonti L, Marchetti P, Lammert E: **Age- and diet-dependent requirement of DJ-1 for glucose homeostasis in mice with implications for human type 2 diabetes.** *J Mol Cell Biol* 2012, **4:**221-230.

15. Cao J, Lou S, Ying M, Yang B: **DJ-1 as a human oncogene and potential therapeutic target.** *Biochem Pharmacol* 2015, **93:**241-250.

16. Hanagasi HA, Giri A, Kartal E, Guven G, Bilgic B, Hauser AK, Emre M, Heutink P, Basak N, Gasser T, et al: **A novel homozygous DJ1 mutation causes parkinsonism and ALS in a Turkish family.** *Parkinsonism Relat Disord* 2016, **29:**117-120.

17. Honbou K, Suzuki NN, Horiuchi M, Niki T, Taira T, Ariga H, Inagaki F: **The crystal structure of DJ-1, a protein related to male fertility and Parkinson's disease.** *J Biol Chem* 2003, **278:**31380-31384.

18. Wilson MA: **The role of cysteine oxidation in DJ-1 function and dysfunction.** *Antioxidants & redox signaling* 2011, **15:**111-122.

19. Lee JY, Song J, Kwon K, Jang S, Kim C, Baek K, Kim J, Park C: **Human DJ-1 and its homologs are novel glyoxalases.** *Hum Mol Genet* 2012, **21:**3215-3225.

20. Richarme G, Liu C, Mihoub M, Abdallah J, Leger T, Joly N, Liebart JC, Jurkunas UV, Nadal M, Bouloc P, et al: **Guanine glycation repair by DJ-1/Park7 and its bacterial homologs.** *Science* 2017, **357:**208-211.

21. Chen J, Li L, Chin LS: **Parkinson disease protein DJ-1 converts from a zymogen to a protease by carboxyl-terminal cleavage.** *Hum Mol Genet* 2010.

22. Shendelman S, Jonason A, Martinat C, Leete T, Abeliovich A: **DJ-1 is a redox-dependent molecular chaperone that inhibits alpha-synuclein aggregate formation.** *PLoS Biol* 2004, **2:**e362.

23. Zhou W, Zhu M, Wilson MA, Petsko GA, Fink AL: **The oxidation state of DJ-1 regulates its chaperone activity toward alpha-synuclein.** *J Mol Biol* 2006, **356:**1036-1048.

24. Kinumi T, Kimata J, Taira T, Ariga H, Niki E: **Cysteine-106 of DJ-1 is the most sensitive cysteine residue to hydrogen peroxide-mediated oxidation in vivo in human umbilical vein endothelial cells.** *Biochem Biophys Res Commun* 2004, **317:**722-728.

25. Yamagishi Y, Saigoh K, Saito Y, Ogawa I, Mitsui Y, Hamada Y, Samukawa M, Suzuki H, Kuwahara M, Hirano M, et al: **Diagnosis of Parkinson's disease and the level of oxidized DJ-1 protein.** *Neurosci Res* 2018, **128:**58-62.

26. Saito Y: **Oxidized DJ-1 as a possible biomarker of Parkinson's disease.** *J Clin Biochem Nutr* 2014, **54:**138-144.

27. Baulac S, LaVoie MJ, Strahle J, Schlossmacher MG, Xia W: **Dimerization of Parkinson's disease-causing DJ-1 and formation of high molecular weight complexes in human brain.** *Mol Cell Neurosci* 2004, **27:**236-246.

28. Meulener MC, Graves CL, Sampathu DM, Armstrong-Gold CE, Bonini NM, Giasson BI: **DJ-1 is present in a large molecular complex in human brain tissue and interacts with alpha-synuclein.** *J Neurochem* 2005, **93:**1524-1532.

29. Nural H, He P, Beach T, Sue L, Xia W, Shen Y: **Dissembled DJ-1 high molecular weight complex in cortex mitochondria from Parkinson's disease patients.** *Mol Neurodegener* 2009, **4:**23.

30. Saito Y, Akazawa-Ogawa Y, Matsumura A, Saigoh K, Itoh S, Sutou K, Kobayashi M, Mita Y, Shichiri M, Hisahara S, et al: **Oxidation and interaction of DJ-1 with 20S proteasome in the erythrocytes of early stage Parkinson's disease patients.** *Sci Rep* 2016, **6:**30793.

31. Cha SS, Jung HI, Jeon H, An YJ, Kim IK, Yun S, Ahn HJ, Chung KC, Lee SH, Suh PG, Kang SO: **Crystal structure of filamentous aggregates of human DJ-1 formed in an inorganic phosphate-dependent manner.** *J Biol Chem* 2008, **283:**34069-34075.

32. Kim MS, Lee S, Yun S, Suh PG, Park J, Cui M, Choi S, Cha SS, Jin W: **Inhibitory effect of tartrate against phosphate-induced DJ-1 aggregation.** *Int J Biol Macromol* 2018, **107:**1650-1658.

33. Aslund A, Sigurdson CJ, Klingstedt T, Grathwohl S, Bolmont T, Dickstein DL, Glimsdal E, Prokop S, Lindgren M, Konradsson P, et al: **Novel pentameric thiophene derivatives**

for in vitro and in vivo optical imaging of a plethora of protein aggregates in cerebral amyloidoses. *ACS Chem Biol* 2009, **4:**673-684.

34. Kiss R, Zhu M, Jojart B, Czajlik A, Solti K, Forizs B, Nagy E, Zsila F, Beke-Somfai T, Toth G: **Structural features of human DJ-1 in distinct Cys106 oxidative states and their relevance to its loss of function in disease.** *Biochim Biophys Acta* 2017, **1861:**2619-2629.

35. Micsonai A, Wien F, Kernya L, Lee YH, Goto Y, Refregiers M, Kardos J: **Accurate secondary structure prediction and fold recognition for circular dichroism spectroscopy.** *Proc Natl Acad Sci U S A* 2015, **112:**E3095-3103.

36. Chan FT, Kaminski Schierle GS, Kumita JR, Bertoncini CW, Dobson CM, Kaminski CF: **Protein amyloids develop an intrinsic fluorescence signature during aggregation.** *Analyst* 2013, **138:**2156-2162.

37. Conway KA, Harper JD, Lansbury PT, Jr.: **Fibrils formed in vitro from alpha-synuclein and two mutant forms linked to Parkinson's disease are typical amyloid.** *Biochemistry* 2000, **39:**2552-2563.

38. Hulleman JD, Mirzaei H, Guigard E, Taylor KL, Ray SS, Kay CM, Regnier FE, Rochet JC: **Destabilization of DJ-1 by familial substitution and oxidative modifications: implications for Parkinson's disease.** *Biochemistry* 2007, **46:**5776-5789.

39. Meulener MC, Graves CL, Sampathu DM, Armstrong-Gold CE, Bonini NM, Giasson BI: **DJ-1 is present in a large molecular complex in human brain tissue and interacts with alpha-synuclein.** *Journal of neurochemistry* 2005, **93:**1524-1532.

40. Saito Y, Miyasaka T, Hatsuta H, Takahashi-Niki K, Hayashi K, Mita Y, Kusano-Arai O, Iwanari H, Ariga H, Hamakubo T, et al: **Immunostaining of oxidized DJ-1 in human and mouse brains.** *J Neuropathol Exp Neurol* 2014, **73:**714-728.

41. Rizzu P, Hinkle DA, Zhukareva V, Bonifati V, Severijnen LA, Martinez D, Ravid R, Kamphorst W, Eberwine JH, Lee VM, et al: **DJ-1 colocalizes with tau inclusions: a link between parkinsonism and dementia.** *Annals of neurology* 2004, **55:**113-118.

42. Drummond E, Nayak S, Faustin A, Pires G, Hickman RA, Askenazi M, Cohen M, Haldiman T, Kim C, Han X, et al: **Proteomic differences in amyloid plaques in rapidly progressive and sporadic Alzheimer's disease.** *Acta Neuropathol* 2017, **133:**933-954.

43. Moore DJ, Zhang L, Troncoso J, Lee MK, Hattori N, Mizuno Y, Dawson TM, Dawson VL: **Association of DJ-1 and parkin mediated by pathogenic DJ-1 mutations and oxidative stress.** *Hum Mol Genet* 2005, **14:**71-84.

44. Smith N, Wilson MA: **Structural Biology of the DJ-1 Superfamily.** *Adv Exp Med Biol* 2017, **1037:**5-24.

45. Herrera FE, Zucchelli S, Jezierska A, Lavina ZS, Gustincich S, Carloni P: **On the oligomeric state of DJ-1 protein and its mutants associated with Parkinson Disease. A combined computational and in vitro study.** *J Biol Chem* 2007, **282:**24905-24914.

46. Ramsey CP, Giasson BI: **L10p and P158DEL DJ-1 mutations cause protein instability, aggregation, and dimerization impairments.** *J Neurosci Res* 2010, **88:**3111-3124.

Figure titles and legends

Fig. 1. Homodimeric DJ-1 formed ThioT positive fibril-like aggregates when incubated *in vitro*. The hydrodynamic diameter of DJ-1 as a function of time in (a) phosphate and (b) Tris-buffers observed by DLS. In each figure, DJ-1$_{Cys106(S-)}$ (black squares), DJ-1$_{Cys106(SO2-)}$ (red circles) and DJ-1$_{Cys106(SO3-)}$ (blue triangles) and BSA (turquoise blue used as a control protein), are shown. (c) Quantification of loss of homodimeric DJ-1 due to DJ-1 aggregate formation as a function of time in phosphate buffer by ultracentrifugation. Fluoresence intensity of (d) Thioflavin T after 7 days of incubation in phosphate buffer. Fluoresence intensity of (e) pFTAA and (f) intrinsic fluorescence of DJ-1 as a function of time in phosphate buffer. TEM images of (g) DJ-1$_{Cys106(S-)}$, (h) DJ-1$_{Cys106(SO2-)}$, and (i) DJ-1$_{Cys106(SO3-)}$ samples after 5 days of incubation in phosphate buffer. All figures, correspond to experiments in which protein samples were incubated in quiescent conditions at 30 μM, 37°C and pH = 7.4 for 5 days in phosphate buffer solution except for (b) where Tris-buffer was used.

Fig. 2. Homodimeric DJ-1 misfolds and forms soluble aggregate with a high parallel β-sheet structural content when incubated *in vitro*. CD spectra of (a) DJ-1$_{Cys106(S-)}$, (b) DJ-1$_{Cys106(SO2-)}$, (c) DJ-1$_{Cys106(SO3-)}$, (g) BSA samples observed at the start of incubation before ultracentrifugation (blue squares), following incubation of the supernatants after ultracentrifugation (red line), and of the pellets after ultracentrifugation (blue line). Second derivative of the FT-IR spectra for (d) DJ-1$_{Cys106(S-)}$, (e) DJ-1$_{Cys106(SO2-)}$, and (f) DJ-1$_{Cys106(SO3-)}$ and (h) BSA samples at the start of (red line) and after incubation (blue line). The CD and FT-IR spectra of BSA protein did not change significantly after incubation. All figures correspond to

experiments in which protein samples were incubated in quiescent conditions at 30 μM for 5 days at 37°C and pH = 7.4 in phosphate buffer solution.

Fig. 3. The aggregation of DJ-1 results in a loss of its glyoxalase function. (a) Glyoxalase activity of DJ-1$_{Cys106(S-)}$ in its homodimeric state (DJ-1 control) and after incubation for 5 days at 37$_o$C in quiescent conditions (aggregated DJ-1), and for inactivated DJ-1$_{Cys106(S-)}$ treated with iodoacetamide (DJ-1 + IAA), as a positive control, in an MGO depletion assay in phosphate buffer at 22$_o$C and pH = 7.4. Separation of DJ-1 multimeric states after incubation of DJ-1 homodimers for 24 hours in phosphate buffer, at 37$_o$C and pH = 7.4 by NATIVE PAGE with (b) Coomassie Blue staining and (c) Western Blotting using mAb$_{anti\text{-}oxDJ\text{-}1}$. In each case, samples were DJ-1$_{Cys106(S-)}$ from the start of the incubation (lane 1), DJ-1$_{Cys106(SO2-)}$ from the start of the incubation (lane 2), DJ-1$_{Cys106(SO3-)}$ from the start of the incubation (lane 3), DJ-1$_{Cys106(S-)}$ after incubation (lane 4), DJ-1$_{Cys106(SO2-)}$ after incubation (lane 5), DJ-1$_{Cys106(SO3-)}$ after incubation (lane 6) and DSS cross-linked DJ-1$_{Cys106(SO2-)}$ from the start of the incubation, as a marker for a homodimer state, (lane 7). (d) Schematic representation of hypothized aggregation mechanism of DJ-1 protein.

Fig. 4. Oxidized DJ-1 co-localizes with phospho-α-synuclein and -Tau in the human post-mortem PD brain, and with amyloid plaques and phospho-Tau in post-mortem AD brain. Triple-labeling immunofluorescence (TIF) of PD and aged-matched control tissue from the amygdala with (a) pFTAA, mAb$_{anti\text{-}oxDJ\text{-}1}$, and Hoechst, (b) mAb$_{p\text{-}\alpha syn}$, mAb$_{anti\text{-}oxDJ\text{-}1}$, and Hoechst, (c) mAb$_{p\text{-}Tau}$, mAb$_{anti\text{-}oxDJ\text{-}1}$, and Hoechst. TIF of AD and aged-matched control post-mortem brain tissue taken from the frontal cortex with (d) pFTAA, mAb$_{anti\text{-}oxDJ\text{-}1}$, and

$mAb_{A\beta42}$and (e) pFTAA, $mAb_{anti\text{-}oxDJ\text{-}1}$, $mAb_{p\text{-}Tau}$. (f, g) The intensity of oxDJ-1 and pFTAA expression was quantified in 10 randomly sampled field of view and averaged per patient. Bars represent 10 μm.

Table 1. Estimated secondary structure content, in percentage (%), of DJ-1 samples at the start of incubation and after 5 days of incubation as determined by CD measurements. Secondary structure content analyzes of the CD spectroscopic data was carried out by BeStSel.

Fig. 1

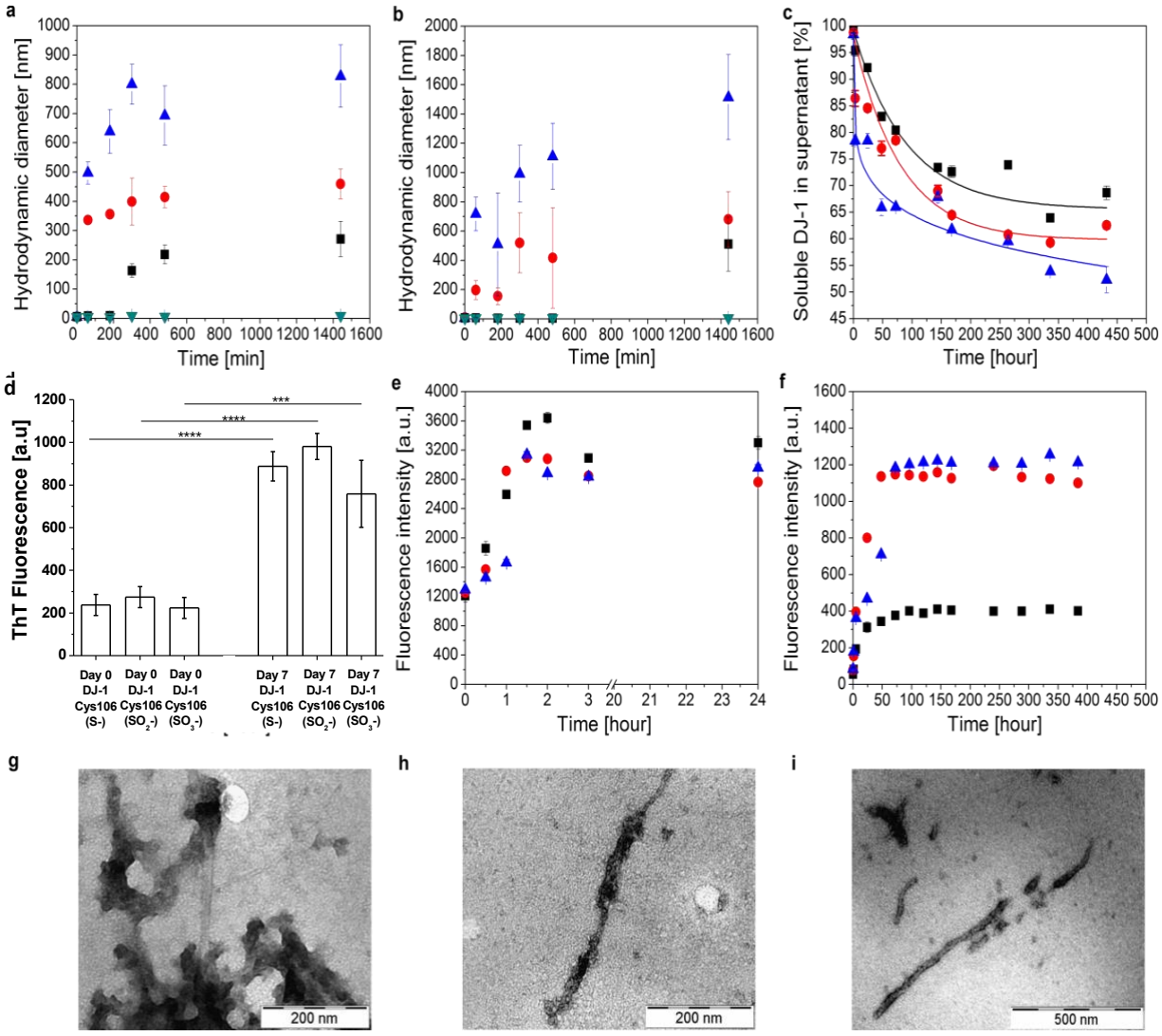
a
Hydrodynamic diameter [nm]
Time [min]
b
Hydrodynamic diameter [nm]
Time [min]
c
Soluble DJ-1 in supernatant [%]
Time [hour]
d
ThT Fluorescence [a.u]
***
****
****
Day 0 DJ-1 Cys106 (S-)
Day 0 DJ-1 Cys106 (SO2-)
Day 0 DJ-1 Cys106 (SO3-)
Day 7 DJ-1 Cys106 (S-)
Day 7 DJ-1 Cys106 (SO2-)
Day 7 DJ-1 Cys106 (SO3-)
e
Fluorescence intensity [a.u.]
Time [hour]
f
Fluorescence intensity [a.u.]
Time [hour]
g
200 nm
h
200 nm
i
500 nm

Fig. 2

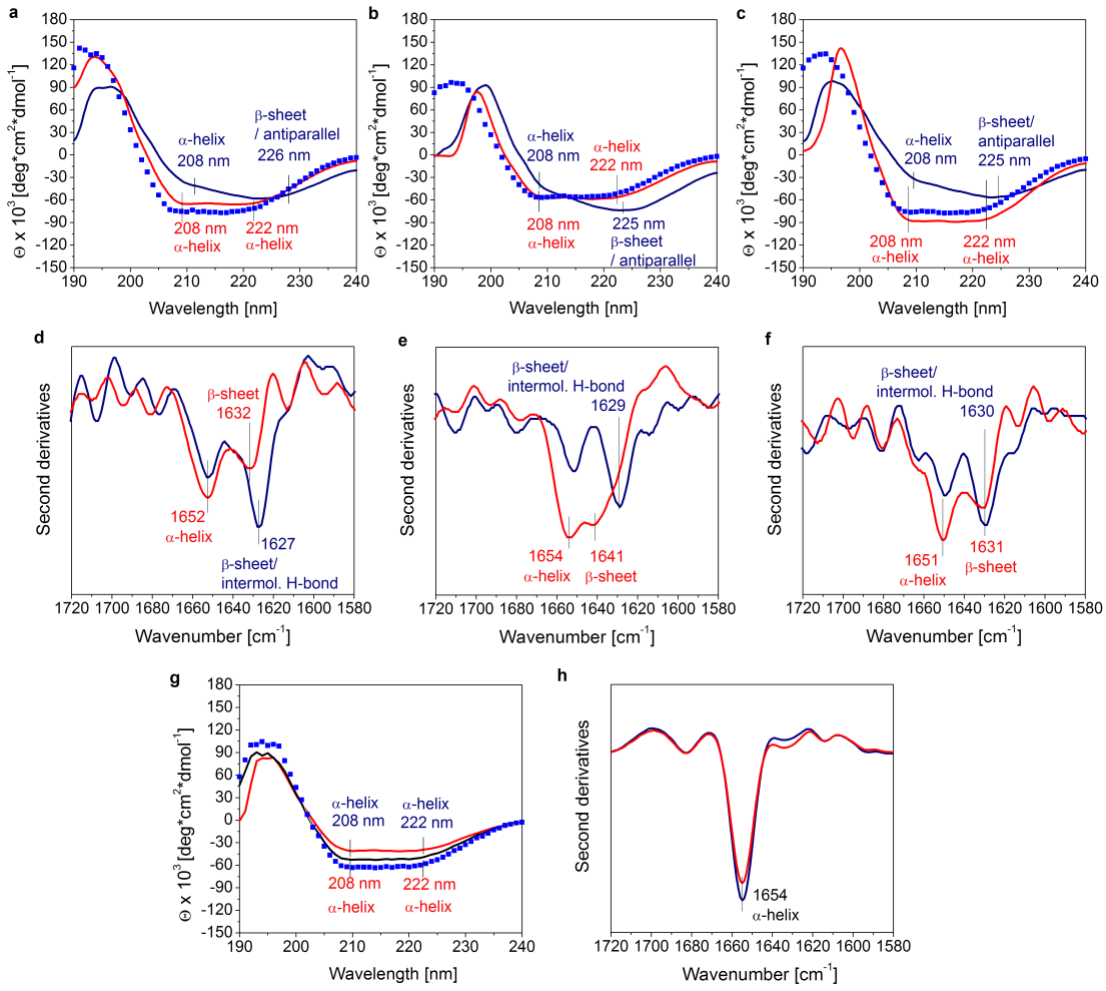
a
b
c
d
e
f
g
h
Θ x 10^3 [deg*cm^2*dmol^-1]
Wavelength [nm]
α-helix
208 nm
β-sheet
/ antiparallel
226 nm
208 nm
α-helix
222 nm
α-helix
222 nm
208 nm
α-helix
225 nm
β-sheet
/ antiparallel
β-sheet/
antiparallel
225 nm
Second derivatives
Wavenumber [cm^-1]
β-sheet
1632
1652
α-helix
1627
β-sheet/
intermol. H-bond
β-sheet/
intermol. H-bond
1629
1654
α-helix
1641
β-sheet
β-sheet/
intermol. H-bond
1630
1651
α-helix
1631
β-sheet
1654
α-helix

Fig. 3.

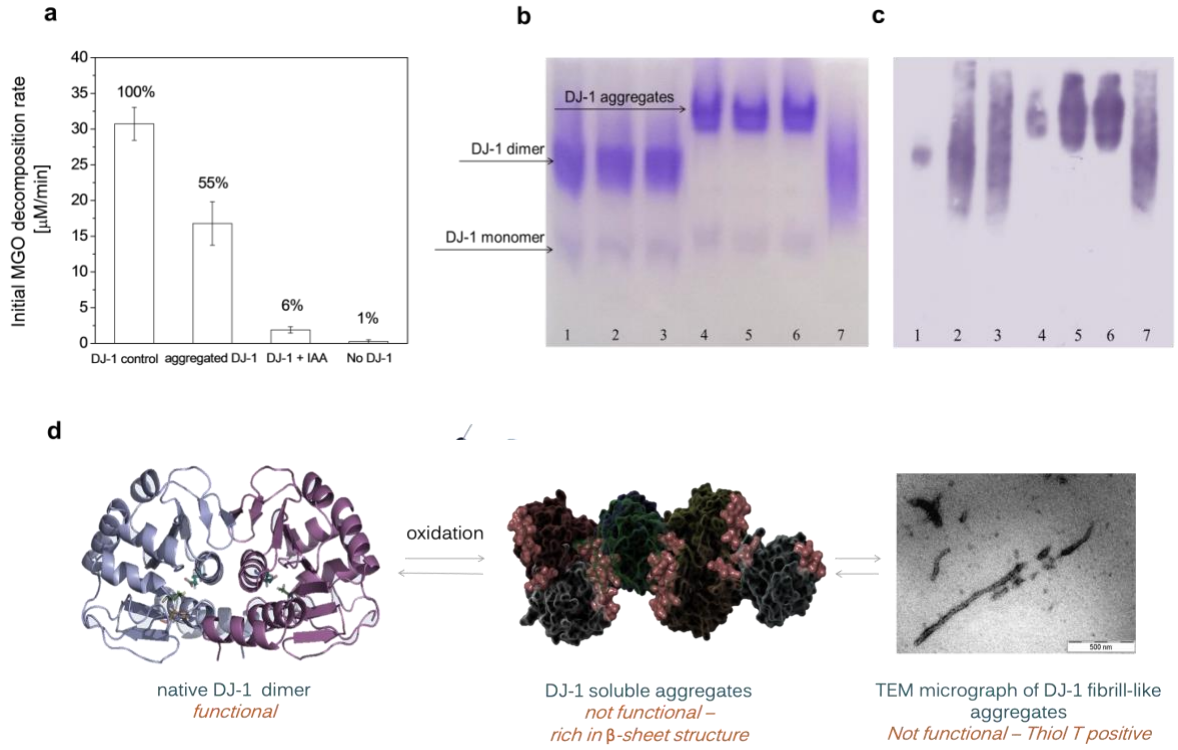
a
b
c
d
Initial MGO decomposition rate [μM/min]
100%
55%
6%
1%
DJ-1 control
aggregated DJ-1
DJ-1 + IAA
No DJ-1
DJ-1 aggregates
DJ-1 dimer
DJ-1 monomer
1 2 3 4 5 6 7
oxidation
native DJ-1 dimer
functional
DJ-1 soluble aggregates
not functional –
rich in β-sheet structure
TEM micrograph of DJ-1 fibrill-like aggregates
Not functional – Thiol T positive

Fig. 4

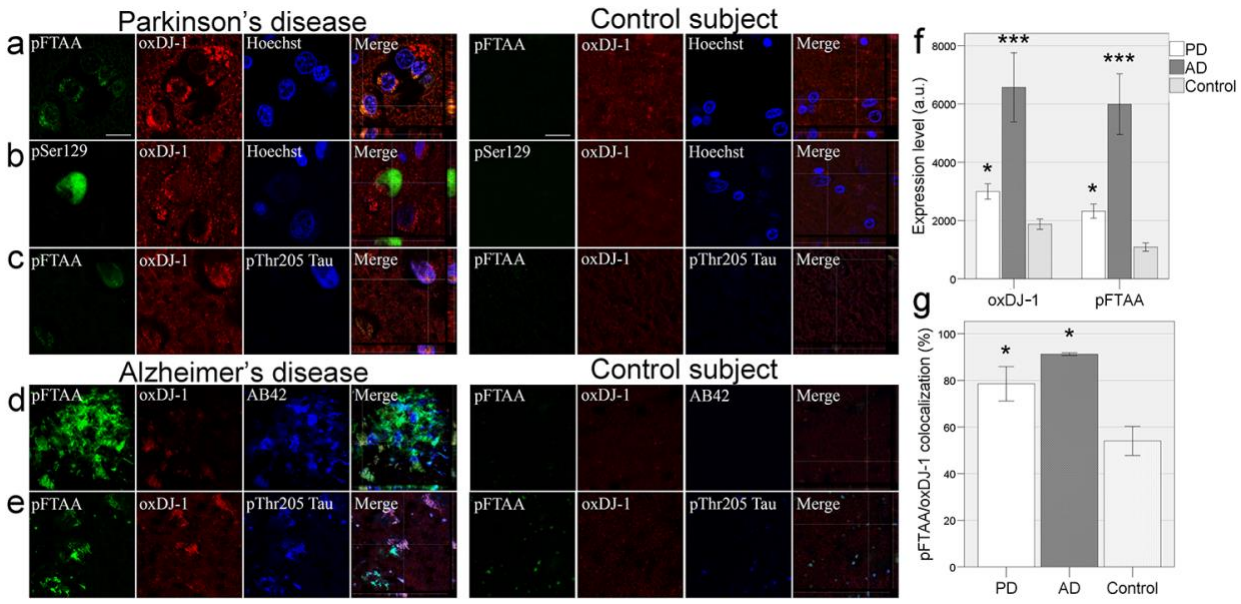
Parkinson's disease
Control subject
a
pFTAA
oxDJ-1
Hoechst
Merge
b
pSer129
c
pThr205 Tau
Alzheimer's disease
d
AB42
e
f
Expression level (a.u.)
PD
AD
Control
oxDJ-1
pFTAA
g
pFTAA/oxDJ-1 colocalization (%)

Table 1. Estimated secondary structure content, in percentage (%), of DJ-1 samples at the start of incubation and after 5 days of incubation as determined by CD measurements. Secondary structure content analyzes of the CD spectroscopic data was carried out by BeStSel.

	Incubation (in days)	α-helix	β-sheet/ parallel	β-sheet/ antiparallel	Turn
DJ-1$_{Cys106(S-)}$					
DJ-1 dimer*	0	45.1	40.1	4	10.8
DJ-1 in supernatant**	5	67	24.7	0	8.3
Aggregated DJ-1***	5	6.8	52.8	26.5	13.9
DJ-1$_{Cys106(SO2-)}$					
DJ-1 dimer*	0	41.1	30.3	17.8	10.8
DJ-1 in supernatant**	5	50.9	22.3	18.6	8.2
Aggregated DJ-1***	5	8.4	40.6	30.9	20.1
DJ-1$_{Cys106(SO3-)}$					
DJ-1 dimer*	0	43.7	27.6	17.1	11.6
DJ-1 in supernatant**	5	54.6	26.7	9	9.7
Aggregated DJ-1***	5	8.7	26.2	51.1	14

* native DJ-1 dimer before start of aggregation, non-aggregated DJ-1 dimer
** DJ-1 dimer in supernatant after aggregation and ultracentrifugation (v = 54,000 rpm)
*** DJ-1 in aggregated rich phase after ultracentrifugation (v = 54,000 rpm)